

An effective route to the additive manufacturing of a mechanically gradient supramolecular polymer nanocomposite structure

Sara Salimi^{a,d}, Aaron M. Graham^b, Yuyang Wu^c, Peihao Song^b, Lewis R. Hart^a, Derek J. Irvine^c, Ricky D. Wildman^c, Clive R. Siviour^b, Wayne Hayes^{a,*}

^a Department of Chemistry, University of Reading, Whiteknights, Reading, RG6 6AD, UK

^b Department of Engineering Science, University of Oxford, Oxford, OX1 3PJ, UK

^c Faculty of Engineering, The University of Nottingham, University Park, Nottingham, NG7 2RD, UK

^d Department of Chemistry and Chemical Biology, McMaster University, 1280 Main St. W., Hamilton, Ontario, L8S 4M1, Canada

ARTICLE INFO

Keywords:

A. polymers-matrix composites
B. Mechanical properties
E. Extrusion
E. 3D printing

ABSTRACT

3D Printing techniques are additive methods of fabricating parts directly from computer-aided designs. Whilst the clearest benefit is the realisation of geometrical freedom, multi-material printing allows the introduction of compositional variation and highly tailored product functionality. The paper reports a proof-of-concept additive manufacturing study to deposit a supramolecular polymer and a complementary organic filler to form composites with gradient composition to enable spatial distribution of mechanical properties and functionality by tuning the number of supramolecular interactions. We use a dual-feed extrusion 3D printing process, with feed stocks based on the supramolecular polymer and its organic composite, delivered at ratios predetermined. This allows for production of a graded specimen with varying filler concentration that dictates the mechanical properties. The printed specimen was inspected under dynamic load in a tensile test using digital image correlation to produce full-field deformation maps, which showed clear differences in deformation in regions with varying compositions, corresponding to the designed-in variations. This approach affords a novel method for printing material with graded mechanical properties which are not currently commercially available or easily accessible, however, the method can potentially be directly translated to the generation of biomaterial-based composites featuring gradients of mechanical properties.

1. Introduction

Additive manufacturing, also known as 3D printing, has made significant advances in recent years in producing functional objects that can see service (Zhu et al., 2022; Jandyal et al., 2022). A key determinant of this progress is the identification and synthesis of advanced materials that are suitable for uses that progress beyond prototyping and allow the design and manufacture of more durable, functional and customised structures (Zhu et al., 2022; Xiao and Kan, 2022). One of the material classes beginning to show promise is supramolecular polymers (Hart et al., 2016; Pekkanen et al., 2017; Rupp et al., 2019; Meurer et al., 2022; Sather et al., 2021). Supramolecular polymers are a class of stimuli-responsive materials which are able to self-assemble into dynamic arrays as a result of highly directional and specific non-covalent interactions. These materials offer a broad range of mechanical properties based on their structure, molecular weight and the recognition

motif (O' et al., 2022). The improvement in the mechanical properties of these materials can be achieved through different methods such as introduction of inorganic/organic fillers (Pedrazzoli and Manas-Zloczower, 2016; Salimi et al., 2019) or incorporation of a UV curable motif, in order to add a secondary reinforcing covalent network (Masuda et al., 2003). The primary effort for developing these materials so far has been on producing systems with high fracture toughness, and this has resulted in considerable improvement of the design and dispersion of fillers within the matrix through, e.g. surface functionalisation in order to promote uniformity (Kim et al., 2016).

An alternative approach to manipulation at the molecular and micro scales, is the exploitation of the *compositional* design freedoms of additive manufacturing. Additive manufacturing is well-known for its geometrical design freedom, i.e., the ability to adopt highly complex shapes without punitive marginal costs, but additive manufacturing also offers the chance to spatially vary the composition of a structure within

* Corresponding author.

E-mail address: w.c.hayes@reading.ac.uk (W. Hayes).

<https://doi.org/10.1016/j.jmbbm.2023.106358>

Received 8 June 2023; Received in revised form 20 December 2023; Accepted 26 December 2023

Available online 29 December 2023

1751-6161/© 2023 The Authors. Published by Elsevier Ltd. This is an open access article under the CC BY license (<http://creativecommons.org/licenses/by/4.0/>).

that shape in a highly controlled manner, (Bracaglia et al., 2017; Li et al., 2020) giving another dimension to design and control of function (He et al., 2020). The combination of 3D printing with an external field such as magnetic field or ultrasound has enabled alignment of fillers during fabrication of polymeric composite parts (Niendorf and Raeymaekers, 2021). Such approaches are often inspired-by-nature designs such as gradient materials observed in squid beaks (Miserez et al., 2008) and byssus threads (Claussen et al., 2012) or Bouligand structures (Greenhall and Raeymaekers, 2017). Generation of mechanically gradient polymers (MGPs) offers a new level of functionality to the polymers (Shen et al., 1972). For example, the role of byssus threads is to provide robust attachment of mussel to rock which faces turbulent sea water. Consequently, in order to minimise the energy imposed on the mussel, these threads are stiffer at the ends and more flexible where it is connected to the mussel's soft body tissue, (Smeathers et al., 1979) but this is difficult to achieve with traditional manufacturing methods. Mechanical gradient polymers allow a new approach to produce shapes and parts with differing mechanical properties within their structure that can be produced by controlled changes in the concentration of the reinforcing component or tailoring the stiffness via the polymer crosslinking density (Claussen et al., 2014). Adopting these approaches enables fabrication of parts that offer specific failure points, (Kokkinis et al., 2018) mode of force distribution or cell adhesion, (Sunyer et al., 2012) based on the design. The composite materials can offer a broad range of application from artificial skin sensors to security tags (Kokkinis et al., 2018). Printing graded materials can also yield scaffolds to benefit tissue culture affording tissues that better resemble the native structure (Bracaglia et al., 2017; Motealleh et al., 2019).

Gradients of material composition have been demonstrated previously, (He et al., 2021; Levato et al., 2020) but these are generally limited to highly digitised variations in the composition. For example, when using extrusion, (Rupp et al., 2021) it is difficult to achieve variation of composition in the case of single material extrusion and it is limited to varying infill to produce a gradient. Inkjet printing has been used to produce gradient structures but is limited frequently to deposition of photocurable materials; the limited scope of such materials affords a limited range of properties (Godleman et al., 2021; Yao et al., 2007). Producing flexible biocompatible images from UV-curable inks can also prove problematic because of residual unreacted monomers which are cytotoxic to living cells and images generated via this method can be prone to aging, frequently losing their elastomeric properties over time. Photocurable systems can also require additional care in storage, handling and processing of the monomers in the light of their oxygen and humidity sensitivities. Commercially available 3D printers are now capable of operating under inert atmosphere, but this approach is limited by factors such as the size of the confinement (Mendes-Felipe et al., 2019).

This paper reports an additive manufacturing approach to generate MGP structures involving the combined use of an extrusion system with a supramolecular polymer composite that can be dosed in a controlled fashion to achieve continuous variation of the polymer composition in the resultant image. Extrusion printing, which can be categorized as a type of direct ink writing, has been used before to generate complex components to enable the study of the effect of internal geometry on the functionality of composite material such as conductivity (Lewis, 2006). Our method is, however, based upon the use of a customised extrusion 3D printer that takes advantage of the temperature sensitive viscosity behaviour of the supramolecular polymer matrix to vary the composition of the composite material ink being printed, allow the introduction of functionality as well as tailor the geometry design (Burattini et al., 2009). Reinforcement of a supramolecular polyurethane (SPU) in order to produce a gradient design was achieved by varying the content of an organic filler in the bulk polymer phase in a controlled manner which will allow for a higher rate of deposition (Shen et al., 1972). Previously, *in situ* production of the bis-urea low molecular weight additive (LMWA) has been shown to be an effective method of reinforcing supramolecular

polyurethane, which also enables tuning of the mechanical properties by differing the content of LMWA in the system (Salimi et al., 2019). By increasing the content of LMWA in the elastomeric supramolecular polyurethane, the resultant material becomes stiffer and less elastomeric. Herein, a high-content reinforced SPU was mixed with a purified SPU in well-defined volumetric ratios to generate materials with adjustable contents of LMWA (Hopmann and Beyer, 2017).

2. Materials and methods

2.1. Materials

All reagents were purchased from Sigma Aldrich or Alfa Aesar and used as received with the exception of Krasol HLBH-P2000 (M_w as received = 2 kg mol^{-1}) [hydrogenated poly (butadiene)] which was supplied by TOTAL Cray Valley. Solvents were purchased from Stuart Scientific and used as received. Tetrahydrofuran (THF) was distilled from sodium and benzophenone prior to use, where anhydrous THF was needed. The synthetic procedure used to afford the SPU material followed the report by Hayes and co-workers to yield a material with the following molecular weight characteristics (as determined by GPC analysis): $M_n = 9000 \text{ g mol}^{-1}$, $M_w = 12200 \text{ g mol}^{-1}$, $\bar{D} = 1.39$ (Salimi et al., 2019).

2.2. Instrumentation

The extrusion system employed in this study (see Fig. 1) was modified from a LulzBot TAZ6 printer (FAME 3D, Fargo, North Dakota, USA) integrated with a high precision volumetric dosing unit (Preeflow eco-DUO450 two-component mixing dispenser, ViscoTec). Subsequently, a home-built feed supplying system pneumatically transported the reagent mixtures from the Optimum® syringe barrels to the dosing unit by pressurised nitrogen (3 bar). Feeds of the inks (see below) from both syringe barrels were then driven by a screw pump inside the dosing unit to efficiently mix the components. The dosing system used was Preeflow™ eco CONTROL EC200 DUO with eco DUE 450 dispenser equipped with a Groß static mixer set. This dosing system was designed to allow mixing ratios from 1.00:1.00 to 9.00:1.00. A speed mixer Dual Asymmetric Centrifuge DAC 400.1 mixer FVZ was used to homogenise the plasticiser solvent and the SPUs.

The rheological analysis for determination of LVER and yield stress was carried out using a Kinexus Pro rheometer equipped with a 40 mm geometry parallel plate at constant temperature (25°C); the linear viscoelastic region (LEVR) for each formulation was determined at a

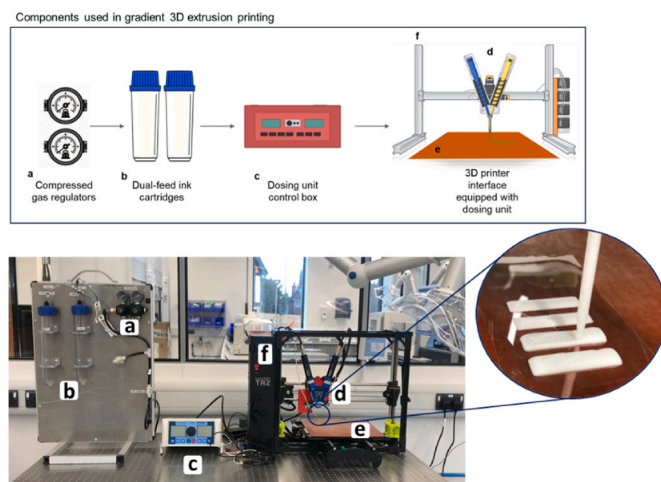


Fig. 1. Picture of the 3D extrusion printer and a schematic of this equipment. Each component of the setting is labelled accordingly.

monotonic strain loading between 0.01% and 1000% and the moduli were monitored. Then, under oscillatory stress conditions at 5 Hz a rheological experiment was carried out on the inks to measure the change in moduli. The shear viscosity rheological measurement was performed using an Anton-Paar Physica MCR302 Rheometer, in oscillatory shear equipped with a 25 mm parallel plate geometry and samples were heated at 2 °C.min⁻¹.

2.3. Formulation of SPU inks

The materials were plasticised using EtOAc, 0.4 mL and 0.5 mL of the solvent was used per gram of material for SPU1 and RSPU-15%, respectively. The solvent was added to the polymer in a mixer container and was left overnight. A Dual Asymmetric Centrifuge DAC 400.1 mixer FVZ was used to homogenise the plasticiser solvent and the SPUs for 8 min at 2500 rpm which resulted in a paste like ink. Each of these materials was loaded in the printer barrels separately as printing feeds. Following the loading of the inks into the printer cartridges and the mixer, the dosing unit was calibrated by volume of each material.

2.4. Printing method

The bar shape 3D design was entered into the CURA-Lulzbot v3.6.20 software and the GCode produced using parameters as follows: 20% zigzag infill, 1 mm layer thickness at the speed of 15 mm.S⁻¹. A nozzle with 1 mm in diameter was used and the print bed was held at ambient temperature. The generated GCode was then modified so that the sample was printed between X177.5 to X102.5 between Y143.5 to Y136.5 with regular pauses in printing every 5 mm. The new GCode was transferred to the printer by SD card to print the MGPs.

2.5. Digital image correlation analysis

Specimens were speckled using a black water-based paint and airbrush, with the white background provided by the natural colour of the specimen. The speckles were produced by pressing a mesh of known pore size against the specimen before spraying both the mesh and the specimen, and then removing the mesh once the paint had dried. Images were recorded using a Pointgrey GS3-U3-41C6M-C and the data was processed using the digital image correlation (DIC) software MatchID 2D DIC, version 2021.1.2. Table 1 shows the parameters used to perform the analysis.

Table 1
Detailed DIC analysis parameters.

Hardware parameters		Analysis parameters	
Image resolution	400 × 2824 px	Image filtering	Gaussing filter, 55 px kernal
Lens	60 mm Nikon	Subset size	31 px/1.31 mm
Aperture	f/4	Step size	4 px
Field of view	16.9 × 119.4 mm	Subset shape	Irregular quadrangle
Image scale	23.64 px/mm	function	
Image format	TIF, 16 bit greyscale	Matching criterion	Zero-normalised sum of square differences (ZNSSD)
Greyscale noise	0.639%	Interpolant	Bi-cubic spline
Average speckle size	3.9 px/0.165 mm	Strain window	11 datapoints
Imaging rate	7 Hz	Strain interpolant	Q8
		Virtual Strain Gauge size	71 px
		Strain formulation	Greene-Lagrange

3. Results and discussion

3.1. Synthesis and formulation of polyurethane inks

The elastomer SPU1 and its reinforced analogues RSPU-15% featuring a low molecular weight organic filler with known properties (Salimi et al., 2019) are shown in Fig. 2. It has been shown that the incorporation of the corresponding LMWA improves the mechanical properties of the supramolecular SPU1 by increasing the concentration of hydrogen bonding introduced through the bisurea LMWA (Salimi et al., 2019). The reinforced analogue material containing 15 wt% of corresponding LMWA (RSPU-15%) was synthesised as the stiffest material which is still capable of forming a film yet is not too brittle to be manipulated. Any higher percentage of LMWA resulted in insoluble material unable to form a film. Additionally, SPU1 was synthesised as the elastomeric component by purification from LMWA side product via precipitation (Salimi et al., 2019).

Efficient mixing of materials was needed to enable production of materials with a range of mechanical properties because of the varying concentrations of the LMWA. An extrusion printer with a mixer nozzle head and a controlled dosing system was used for this purpose (see Fig. 1) enabling efficient mixing of SPU1 and RSPU-15% to generate varied wt% of LMWA in a precise fashion. This printing approach thus varies the mechanical properties of the 3D object produced in a gradient manner along one axis as a result of controlled deposition of LMWA and hence its concentration. The dosing unit cannot be heated, therefore, the material itself needed to be plasticised to allow extrusion. To overcome this practical problem, a small volume of ethyl acetate (EtOAc) was used to plasticise the polymers and generate a processable formulation for the printer's setting. Following the loading of the inks into the printer cartridges and the mixer, the dosing unit was calibrated by volume of each material. In brief, the SPU 1 and RSPU-15% materials were first plasticised using very small volumes (<1 mL) of ethyl acetate, allowing the mixtures to soften overnight before homogenising them to yield paste like inks. The change in the physical properties of the material and the consistency of the produced formulated inks is shown in the Supplementary Information (SI) file, Fig. S1. It must be noted that, upon formulation of the inks, the container was kept airtight to prevent evaporation of the small quantities of solvent present (Akterian, 2020).

3.2. Physical characterisation of the ink formulations

To examine the suitability of the formulated inks for 3D printing, the rheological properties of the inks under conditions representing the application of shear during the printing process were determined (Fig. 3). In the light of this analysis, the composite material was deemed suitable for deposition via extrusion 3D printing (Kadival et al., 2023; Kirchmajer et al., 2015; Highley et al., 2015; Townsend et al., 2019; Zhou et al., 2021). To that aim, the linear viscoelastic region (LVER) for each formulation was determined at a monotonic strain loading. Then under constant oscillatory stress a rheological experiment was carried out and the change in moduli is recorded, Fig. 3 shows the result of this experiment. The rheological studies revealed that upon increasing the shear stress, the viscosity also increases with sudden drops observed at 52 Pa and 51 Pa (SPU1 and RSPU-15%, respectively) correlating to the yield stress of the inks. This necessitates printing at lower shear stress to prevent viscosity increases as this can hinder the flow of the ink. Therefore, a static mixer at the nozzle was employed.

After performing a short 3D printing test of the material, it was found that the plasticised SPU inks exhibited some degree of wetting upon deposition on the print bed. One solution to minimise the wetting effect and maintain the printed structure intact was to heat the print bed moderately to increase the solvent evaporation rate. However, if the temperature of the print bed was set too high the material would also soften and deform. To investigate the viscosity profile of the inks at elevated temperatures, another rheological investigation proved

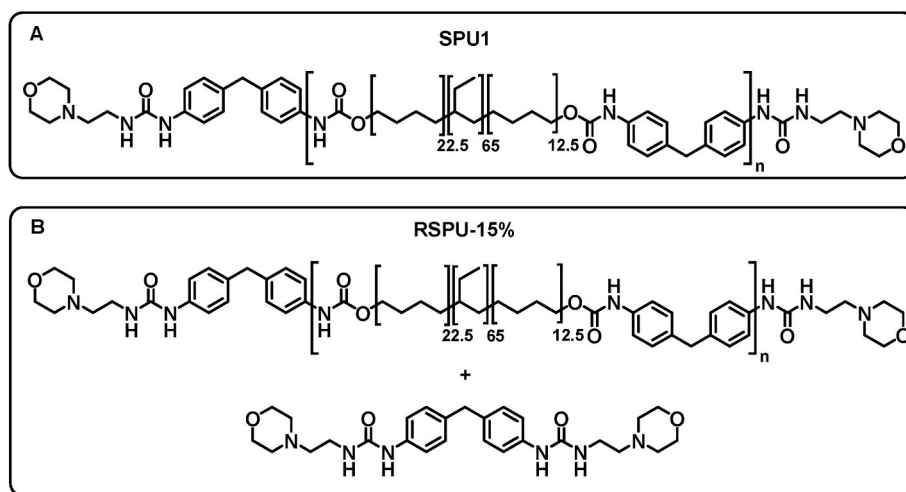


Fig. 2. The chemical structures of A) SPU1 and B) the reinforced system RSPU-15% used to produce an MGP.

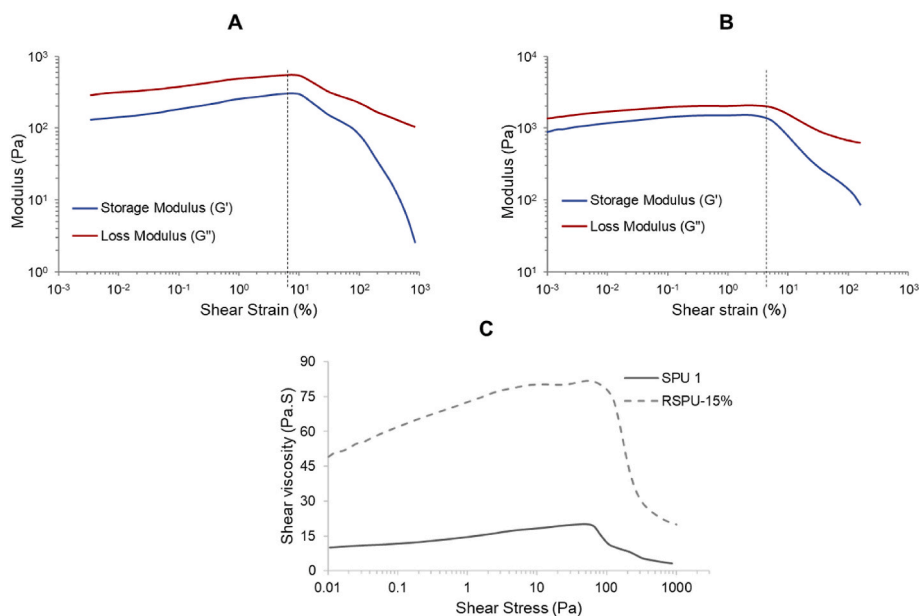


Fig. 3. Top: LVER determination obtained with monotonically applied load A) SPU1 B) RSPU-15% and C) showing the changes of viscosity by shear stress applied at 5 Hz. The drops observed in the bottom graph represents the yield stress of the inks. The graphs are representative of three repeat experiments.

beneficial (Fig. 4). As expected, as the temperature was increased the viscosity of the inks decreased. The decrease was steeper at lower temperatures because of the presence of solvent; the small shear applied by the instrument was able to dissociate the intermolecular interactions in the polymer network. The overall decrease of viscosity can be explained by the fact that the dissociation of the supramolecular interactions outweighs the solvent evaporation effect on viscosity of the ink. In addition, the significant effect of dissociation of supramolecular interactions can be observed by comparing the viscosity profiles of RSPU-15% and SPU1. The drop in viscosity of RSPU-15% is steeper since the concentration of supramolecular assembly motif is higher when compared to the pure SPU1. Consequently, based on these findings, heating the print bed did not prove to be an efficient and practical approach for the prevention of the wetting effect since the material viscosity decreases at elevated temperatures and the image will deform. Therefore, attention turned to optimising other printing settings to avoid the detrimental image deformation.

3.3. 3D printing of the mechanically gradient part

In order to print an MGP part, a bar shape with a varying composition along the longitudinal direction was chosen as a test piece. To that aim, the file of the 3D structure of the design in.stl format was imported into the CURA-Lulzbot. The optimised settings for printing were identified experimentally and are shown in Table 1. Using these settings, the bar design was sliced and a layer-by-layer pattern including the printing path was generated (see Fig. 5A).

A continuous infill pattern was needed to generate a smoother gradient within the part, which meant the nozzle must continuously print rather than printing a line-by-line pattern. Therefore, a zigzag pattern was selected with 20% concentration (a factor of the pattern density) was selected. A value of 20% was found experimentally to be the optimum concentration with minimum line overlap considering the wetting effect outlined above. This parameter represents the distance between the printing line which should be determined experimentally based on the thickness of the filament and the swelling of the ink material as well as the optimum overlapping for a quality print.

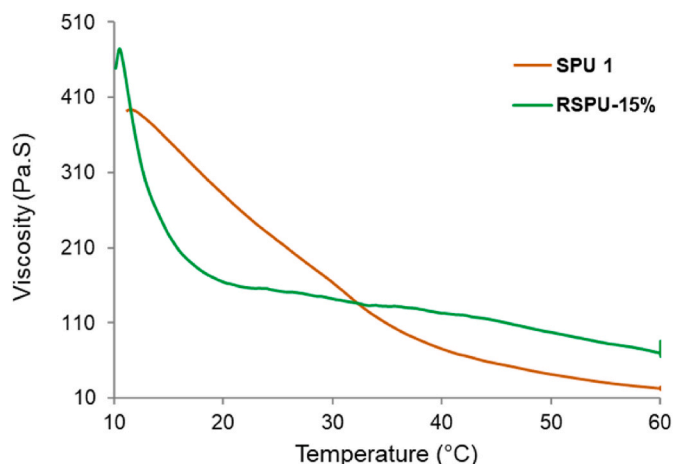


Fig. 4. The viscosity profile of the plasticised inks vs. temperature. The graph obtained at an oscillatory shear experiment with a temperature ramp of $2^{\circ}\text{C}.\text{min}^{-1}$.

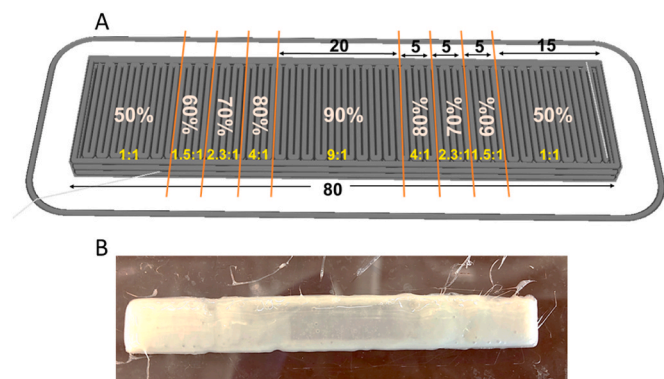


Fig. 5. A) The sliced 3D bar design with CURA illustrating the ratio and percentage of SPU1 to RSPU-15% required to generate the desired MGP (numbers in black are in mm). B) Picture of a printed MGP bar generated in semi-automatic fashion.

The printer was controlled via two different systems: the movement and the dosing unit. The movement of the nozzle was controlled by the CURA software independently from the dosing unit. However, the dosing unit was independent from the CURA software and thus in this proof-of-concept study any change in component ratio currently had to be done manually, though in future it will be possible to automate. To enable varying of the ratio of the materials during a change of location, the movement of the nozzle was paused to allow adjustment of the molar ratio in the dosing system. The printing was then resumed, and the process repeated until printing was complete. The dosing unit can produce mixing ratios of feed materials A and B ranging from 9.00:1.00 to 1.00:1.00. The simple 3D bar design chosen was sliced in CURA and the suitable GCode thus generated. Fig. 5A shows an illustration of the generated GCode in CURA (the grey lined shape) as well as the orange lines which determine the coordinates where the stop command was applied. This figure also indicates the ratios and the corresponding percentages of the SPU1 to RSPU-15% employed in the dosing unit.

The prepared inks were pushed to the dosing system using compressed air. The dosing system can be programmed such that it controls the amount of each ink to be deposited. The dosing was controlled by a combination of gas air pressure and a secondary rotor arm unit. Precision dosing was achieved employing a suckback function to prevent any leakage from the nozzle. The inks were mixed in a static Groß mixer head and subsequently deposited onto acetate sheets on the print bed. Therefore, adjusting the ratio of ink A from printhead A to ink B from

printhead B during the printing on the dosing unit allows production of a gradient material in a continuous manner (see Fig. 5B).

In addition to optimisation of the printer's setting, the dosing unit parameters had to be optimised to achieve a steady filament-like withdrawal of the material from the nozzle. To that aim the parameters were experimentally determined; the flow rate speed of 0.8 mL min^{-1} and a suck back of 0.2 mL at 3.00 mL min^{-1} was employed to obtain a clean stop at the end of the deposition of each composition. The modified GCode was then sent to the printer and the skirt and walls were printed at 1.00:1.00 ratio. When the printhead stopped moving, the dosing was paused by the user, a new ratio set, and the nozzle was flushed carefully to ensure withdrawal of the new composition. Printing was then resumed. This process was continued until the printing of the desired object was complete. Four bars ($80 \times 7 \times 3\text{ mm}$) of the MGP were printed following the same procedure to provide enough repeats for subsequent mechanical properties analysis. Fig. 5B shows a MGP bar printed with this method, as evident from this image, the middle of the bar is composed of softer material (90%) and it gradually becomes less translucent nearer the edges, where the composition is 1:1.

These printed MGP bars were then left at room temperature for 2 days to dry slowly and were then put into a vacuum oven held at 40°C overnight to ensure the samples were totally dry for subsequent mechanical analysis. In order to study the difference in mechanical properties of each composition separately, which can be then correlated to the mechanical properties of the sections within the MGP bar, 4 bars ($40 \times 10 \times 2\text{ mm}$) of each composition were printed for tensile testing. The printed bars were dried following the same procedure as the printed MGP bars.

3.4. Mechanical analysis of the printed samples

After drying the printed bars of each composition suitable for tensile testing, the parts were placed in freezer for a few minutes and were then peeled from the sheet. Since ethyl acetate has a relatively low boiling point (77°C) and high vapour pressure (9.70 kPa at 20°C), it exhibits high specific surface evaporation (9.3 m s^{-1}) (Akterian, 2020). As a result of quick evaporation of the organic solvent in ambient condition, bubbles were generated within the printed bars, despite not heating the samples.

After peeling the samples of individual compositions, they were subjected to tensile testing in order to illustrate the change in tensile properties by varying the feed ratio through testing the bars of each composition. The bars were secured between grips of the tensile testing machine and pulled at a rate of 10 mm min^{-1} . The experiment was repeated three times for each composition and the stress vs. strain was recorded for each sample. The tensile properties of these bars were

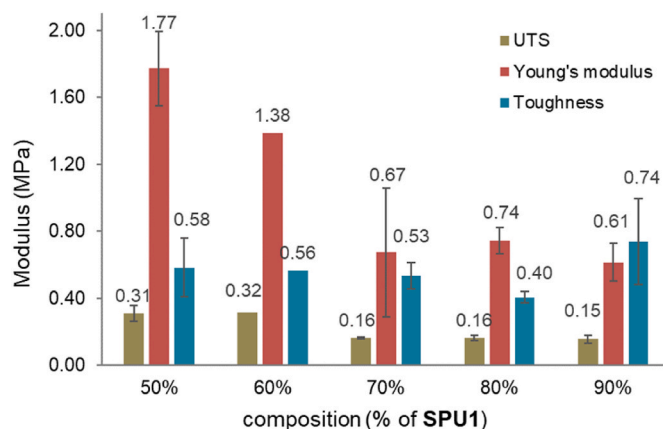


Fig. 6. Calculated tensile properties of different compositions of SPU1 to RSPU-15%. Error bars are standard deviation of three repeat experiments.

calculated based on the data collected and the results are shown in Fig. 6. The X-axis shows the composition percentage of feed A (SPU1) in the sample. Regarding the ultimate tensile strength, by increasing the content of SPU1 (which in turn decreases the amount of LMWA in the formulation) a downward trend was observed. Likewise, upon decreasing the LMWA content, the Young's modulus also decreases, which is indicative of an increase in the elastomeric nature of the material. However, interestingly the modulus of toughness, which was calculated based on the area under each stress-strain curve, remained almost unchanged within the range of error. This can be explained by the decrease in UTS while the elasticity increased upon increasing of the composition percentage of SPU1. It must be noted that the relatively large error bars originate from the fact that the tested specimens did contain a few small bubbles which led to minor variability of the tensile properties of these samples.

3.5. Digital image correlation of the printed MGP

After establishing the variation of mechanical properties for different compositions of the mixed materials, their behaviour was explored within a single graded sample. This was achieved by using digital image correlation (DIC) to map the displacement fields across the specimen surface (Kokkinis et al., 2018). DIC tracks the full-field displacement of a random speckle pattern applied to the specimen surface from photographs of the specimen taken during the experiment. One advantage of the DIC technique is that it can examine the whole surface, rather than collecting a single point (Hensley et al., 2017). Additionally, since the method involves taking photos/videos of the specimen and correlating the movement of the points to strain, a visual understanding of the full-field strain map can be obtained. Fig. S2 in the SI shows a speckled sample of a printed MGP. The speckles were produced by airbrushing the sample with paint using mesh against the sample. However, while the speckle size was a highly uniform 3.9 pixel on smooth sections of the specimen, some sections lost correlation early within this test because of extremely high local strains arising from bubbles present in the sample.

To perform the experiment, a speckled specimen was tested in a commercial screw-driven machine (Instron 5582) equipped with a 1 kN load cell. The applied deformation rate was 20 mm min^{-1} . A digital camera was used to image the specimen and was synchronised to the test machine. The light source was polarised at 0° , and a linear polarising filter at 90° was placed over the lens. This eliminated most spectral reflections from the specimen surface, reducing glare and improving the quality of the images, see Fig. S3 and Table 2 for the experimental set up. Several reference images were taken, and the pixel:mm scale was calibrated at the beginning of the experiment. Once the experiment began, images were taken at 7 Hz.

As a result of the large final strains and displacements, the image changed significantly throughout the test. In order to cope with this change without loss of correlation, the DIC analysis was performed by updating the reference image with each frame instead of comparing each frame to the reference frame. This resulted in a significantly more robust DIC formulation, but at the cost of slightly higher error. Fig. 7 illustrates a typical result from the DIC analysis, colours indicate the strain field in the specimen. Interestingly, it was possible to observe the presence of the subsurface bubbles via their effect on the strain field long before necking or yielding occurred. Whilst the banding shown in Fig. 7 appears to be visually similar to the banding caused by aliasing when using DIC to measure deformation fields, this banding is distinct from that effect, and is caused by underlying bubbles in the structure of the specimen. As such, the strain bands shown are a representative of a real effect, rather than an experimental artefact. Figure 7 shows that the specimen experiences larger strains in the centre, where there is lower concentration of LMWA and hence the material is more elastomeric. Moving towards the top/bottom of the sample, where the composition is 50% of SPU1 and RSPU-15%, the material is relatively stiffer and therefore elongates less. However, it should be noted that, as mentioned

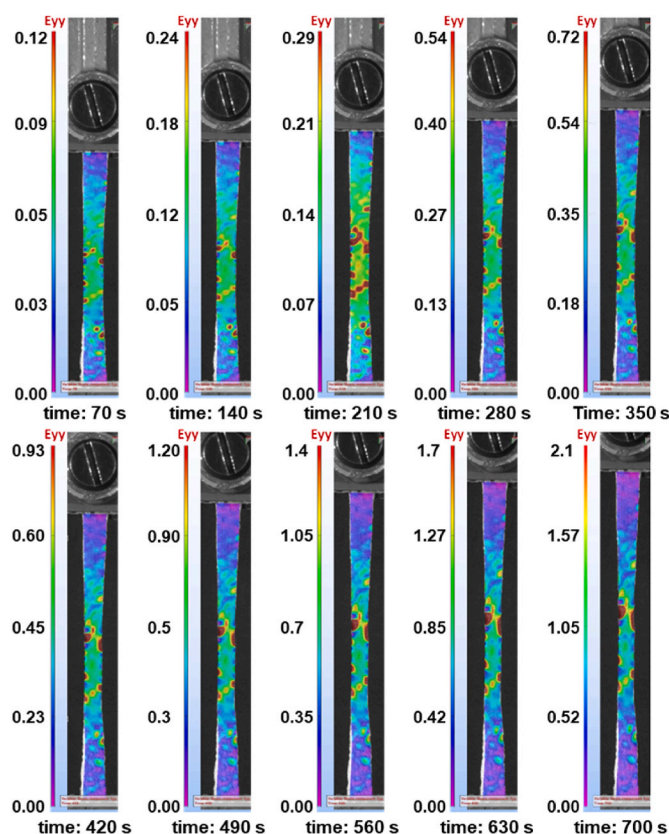


Fig. 7. Strain field calculations in the specimen for different levels of stress during loading, showing strains in the vertical direction (Eyy). Note that the colour bar range is different for each image. The upper bound of each colour bar was set to 3 standard deviations above the mean strain value. Images are recorded every 10 s with select examples shown above.

previously, since the specimen contain bubbles, some areas of higher strain can be seen in the stiff regions of the sample.

In order to further quantify these effects, strain-time data were obtained from the images at a number of points along the specimen, Fig. 8. These data are again consistent with the composition of the material, with larger strains in the centre. The strain analysis reveals different mechanical properties along the sample at different compositions, relative to the concentration of the organic filler at the prospective points. For example, point number 1 with 50% composition (i.e. the stiffest composition) experiences $11 \times$ higher strain when compared to point number 5 with 90% composition (i.e. the most elastic composition).

4. Conclusions and future work

In this prototype system we have demonstrated the use of organic filler for generating gradient materials using 3D extrusion printing free from UV cross-linkable monomers. By combining extrusion 3D printing with supramolecular chemistry, it has been possible to demonstrate the creation of structures with highly controlled material properties, distributed spatially. The performance of our composite structures has been assessed using DIC, which confirmed that the properties of our structure closely correspond with the designed-in variation of the composition. The approach releases additive manufacturing from only having freedoms of shape, to one of being able to have freedom of composition, all while using engineering materials capable of seeing service. If backed with suitable design software that connects the structure, composition and process, this could lead to being able to design *a priori* and subsequently, manufacture structures that meet a

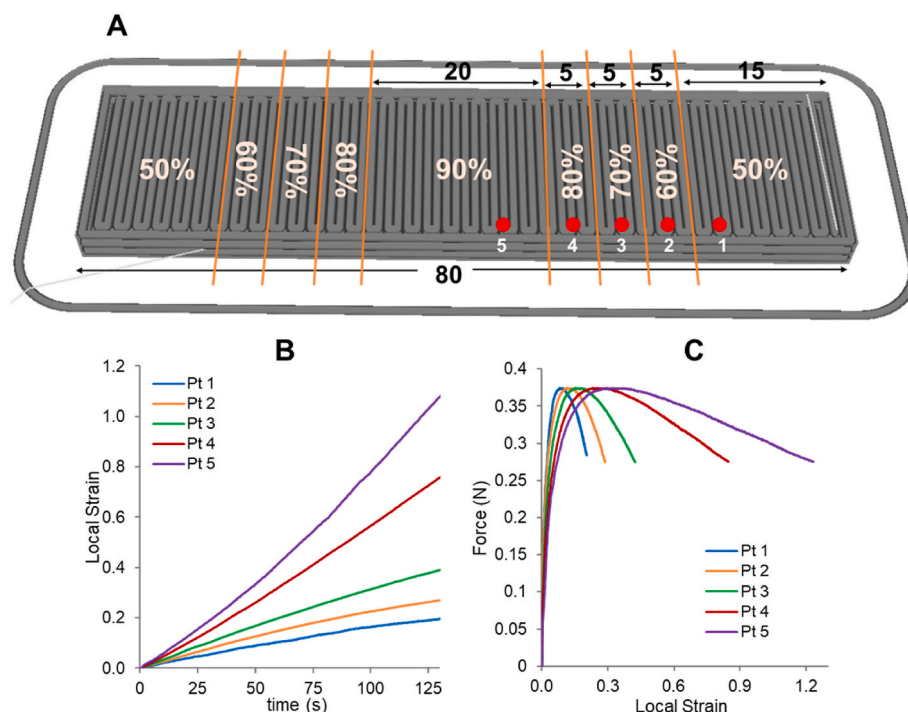


Fig. 8. A) A schematic representation of the MGP sample representing the location of points selected along the sample to screen the strain changes by time (The numbers in black are in mm). B) the strain vs. time graph showing the increase in strain over time. C). changes of strain upon application of force.

highly bespoke need and be highly tailored to a specific requirement. This approach can be translated to the majority of supramolecular polymers by introduction of a complementary LMWA. A clear advantage of using supramolecular polymeric materials and their composites in conjunction with extrusion deposition is the expansion of the material set away from photocurable materials and towards more sophisticated chemistries. A biological example of such an application requiring tailored, personalised and spatially varying properties is artificial skin, requiring the deposition of mechanically varying materials capable of responding to joint movements, combined with conducting elements that provide actuation or sensory awareness of specific joints.

CRediT authorship contribution statement

Sara Salimi: Writing – original draft, Validation, Methodology, Investigation. **Aaron M. Graham:** Writing – review & editing, Methodology, Investigation, Formal analysis. **Yuyang Wu:** Methodology, Investigation. **Peihao Song:** Methodology, Investigation. **Lewis R. Hart:** Methodology, Investigation. **Derek J. Irvine:** Writing – review & editing, Supervision. **Ricky D. Wildman:** Writing – review & editing, Supervision, Methodology. **Clive R. Siviour:** Writing – review & editing, Supervision, Methodology. **Wayne Hayes:** Writing – review & editing, Writing – original draft, Supervision, Project administration, Conceptualization.

Declaration of competing interest

The authors declare that they have no known competing financial interests or personal relationships that could have appeared to influence the work reported in this paper.

Data availability

Data will be made available on request.

Acknowledgments

This work was conducted as part of an EPSRC funded project 'Formulation for 3D Printing' (EP/N024818/1); the extrusion printing system was funded by PPG Inc. The authors would like to acknowledge funding from the University of Reading (ref GS17-025) for postgraduate studentship as well as the Royal Society of Chemistry (M19-1584) for providing a Researchers Mobility Grant in support of SS. Additionally, we would like to acknowledge EPSRC (EP/N024818/1) in support of a postdoctoral fellowships for LRH. The authors would also like to thank Cray Valley for the supply of Krasol HLBH-P2000, the University of Reading for access to analytical instrumentation within the Chemical Analysis Facility. Additionally, the authors would like to thank the Rhodes Trust for their generous support of AMG.

Appendix A. Supplementary data

Supplementary data to this article can be found online at <https://doi.org/10.1016/j.jmbbm.2023.106358>.

The raw/processed data required to reproduce these findings cannot be shared at this time as the data also forms part of an ongoing study.

References

- Akterian, S., 2020. Evaluating the vapour evaporation from the surface of pure organic solvents and their mixtures. *Food Science and Applied Biotechnology* 3, 77–84. <https://doi.org/10.30721/fsab2020.v3.i1.76>.
- Bracaglia, L.G., Smith, B.T., Watson, E., Arumugasaamy, N., Mikos, A.G., Fisher, J.P., 2017. 3D printing for the design and fabrication of polymer-based gradient scaffolds. *Acta Biomater.* 56, 3–13. <https://doi.org/10.1016/j.actbio.2017.03.030>.
- Burattini, S., Colquhoun, H.M., Fox, J., Friedmann, D., Greenland, B.W., Harris, P.J.F., Hayes, W., Mackay, M.E., Rowan, S.J., 2009. A self-repairing, supramolecular polymer system: healability as a consequence of donor–acceptor π - π stacking interactions. *Chem. Commun.* 6717–6719. <https://doi.org/10.1039/b910648k>.
- Claussen, K.U., Scheibel, T., Schmidt, H.W., Giesa, R., 2012. Polymer gradient materials: can nature teach us new tricks? *Macromol. Mater. Eng.* 297, 938–957. <https://doi.org/10.1002/mame.201200032>.
- Claussen, K.U., Giesa, R., Schmidt, H.W., 2014. Longitudinal polymer gradient materials based on crosslinked polymers. *Polymer* 55, 29–38. <https://doi.org/10.1016/j.polymer.2013.11.018>.

- Godleman, J.S., Babra, T.S., Afsar, A., Kyriacou, A., Thompson, M., Harries, J.L., Colquhoun, H.M., Hayes, W., 2021. Functionalised PEGs with photo-dimerisable, anthracenyl end-groups: new UV-curable materials for use in inkjet formulations. *Prog. Org. Coating* 151, 106105. <https://doi.org/10.1016/j.porgcoat.2020.106105>.
- Greenhall, J., Raeymaekers, B., 2017. 3D printing macroscale engineered materials using ultrasound directed self-assembly and stereolithography. *Advanced Materials Technologies* 2, 1700122. <https://doi.org/10.1002/admt.201700122>.
- Hart, L.R., Li, S., Sturgess, C., Wildman, R., Jones, J.R., Hayes, W., 2016. 3D printing of biocompatible supramolecular polymers and their composites. *ACS Appl. Mater. Interfaces* 8, 3115–3122. <https://doi.org/10.1021/acsami.5b10471>.
- He, Y., Foralosso, R., Trindade, G.F., Ilchev, A., Ruiz-Cantu, L., Clark, E.A., Khaled, S., Hague, R.J.M., Tuck, C.F., Rose, F.R.A.J., Mantovani, G., Irvine, D.J., Roberts, C.J., Wildman, R.D., 2020. A reactive prodrug ink formulation strategy for inkjet 3D printing of controlled release dosage forms and implants. *Advanced Therapeutics* 3, 1900187. <https://doi.org/10.1002/adtp.201900187>.
- He, Y., Abdi, M., Trindade, G.F., Begines, B., Dubern, J.F., Prina, E., Hook, A.L., Choong, G.Y.H., Ledesma, J., Tuck, C.J., Rose, F.R.A.J., Hague, R.J.M., Roberts, C.J., De Focatiis, D.S.A., Ashcroft, I.A., Williams, P., Irvine, D.J., Alexander, M.R., Wildman, R.D., 2021. Exploiting generative design for 3D printing of bacterial biofilm resistant composite devices. *Adv. Sci.* 8, 2100249 <https://doi.org/10.1002/advs.202100249>.
- Hensley, S., Christensen, M., Small, S., Archer, D., Lakes, E., Rogge, R., 2017. Digital image correlation techniques for strain measurement in a variety of biomechanical test models. *Acta Bioeng. Biomech.* 19, 187–195. <https://doi.org/10.5277/ABB-00785-2016-04>.
- Highley, C.B., Rodell, C.B., Burdick, J.A., 2015. Direct 3D printing of shear-thinning hydrogels into self-healing hydrogels. *Adv. Mater.* 27, 5075–5079. <https://onlinelibrary.wiley.com/doi/abs/10.1002/adma.201501234>.
- Hopmann, C., Beyer, G., 2017. *Reactive Extrusion Principles and Applications*. John Wiley and Sons.
- Jandyal, A., Chaturvedi, I., Wazir, I., Raina, A., Ul Haq, M.I., 2022. 3D printing – a review of processes, materials and applications in industry 4.0. *Sustainable Operations and Computers* 3, 33–42. <https://doi.org/10.1016/j.susoc.2021.09.004>.
- Kadival, A., Kour, M., Meena, D., Mitra, J., 2023. Extrusion-based 3D food printing: printability assessment and improvement techniques. *Food Bioprocess Technol.* 16, 987–1008. <https://doi.org/10.1007/s11947-022-02931-z>.
- Kim, H., Ko, J., Sohn, D., Ryu, J., Lee, J., Shin, J., 2016. Catechol grafted silica particles for enhanced adhesion to metal by coordinate bond. *Colloids Surf. A Physicochem. Eng. Asp.* 511, 55–63. <https://doi.org/10.1016/j.colsurfa.2016.09.062>.
- Kirchmayer, D.M., Gorkin III, R., inhetPanhuis, M., 2015. An overview of the suitability of hydrogel-forming polymers for extrusion-based 3D-printing. *J. Mater. Chem. B* 3, 4105–4117. <https://doi.org/10.1039/C5TB00393H>.
- Kokkinis, D., Bouville, F., Studart, A.R., 2018. 3D printing of materials with tunable failure via bioinspired mechanical gradients. *Adv. Mater.* 30, 1–9. <https://doi.org/10.1002/adma.201705808>.
- Levato, R., Jungst, T., Scheuring, R.G., Blunk, T., Groll, J., Malda, J., 2020. From shape to function: the next step in bioprinting. *Adv. Mater.* 32, 1906423 <https://doi.org/10.1002/adma.201906423>.
- Lewis, J.A., 2006. Direct ink writing of 3D functional materials. *Adv. Funct. Mater.* 16, 2193–2204. <https://doi.org/10.1002/adfm.200600434>.
- Li, Y., Feng, Z., Hao, L., Huang, L., Xin, C., Wang, Y., Bilotti, E., Essa, K., Zhang, H., Li, Z., Yan, F., Peijs, T., 2020. A review on functionally graded materials and structures via additive manufacturing: from multi-scale design to versatile functional properties. *Advanced Materials Technologies* 5, 1900981. <https://doi.org/10.1002/admt.201900981>.
- Masuda, M., Jonkheijm, P., Sijbesma, R.P., Meijer, E.W., 2003. Photoinitiated polymerization of columnar stacks of self-assembled trialkyl-1,3,5-benzenetricarboxamide derivatives. *J. Am. Chem. Soc.* 125, 15935–15940. <https://doi.org/10.1021/ja037927u>.
- Mendes-Felipe, C., Oliveira, J., Etxebarria, I., Vilas-Vilela, J.L., Lanceros-Mendez, S., 2019. State-of-the-Art and future challenges of UV curable polymer-based smart materials for printing technologies. *Advanced Materials Technologies* 4, 1–16. <https://doi.org/10.1002/admt.201800618>.
- Meurer, J., Kampes, R.H., Bätz, T., Hniopek, J., Müschke, O., Kimmig, J., Zechel, S., Schmitt, M., Popp, J., Hager, M.D., Schubert, U.S., 2022. 3D-Printable shape-memory polymers based on halogen bond interactions. *Adv. Funct. Mater.* 32, 2207313 <https://doi.org/10.1002/adfm.202207313>.
- Miserez, A., Schneberk, T., Sun, C., Zok, F.W., Waite, J.H., 2008. The transition from stiff to compliant materials in squid beaks. *Science* 319, 1816–1819. <https://doi.org/10.1126/science.1154117>.
- Motealleh, A., Çelebi-Saltik, B., Ermis, N., Nowak, S., Khademhosseini, A., Kehr, N.S., 2019. 3D printing of step-gradient nanocomposite hydrogels for controlled cell migration. *Biofabrication* 11, 045015. <https://doi.org/10.1088/1758-5090/ab3582>.
- Niendorf, K., Raeymaekers, B., 2021. Additive manufacturing of polymer matrix composite materials with aligned or organized filler material: a review. *Adv. Eng. Mater.* 23, 2001002 <https://doi.org/10.1002/adem.202001002>.
- O'Donnell, A.D., Salimi, S., Hart, L.R., Babra, T.S., Greenland, B.W., Hayes, W., 2022. Applications of supramolecular polymer networks. *React. Funct. Polym.* 172, 105209 <https://doi.org/10.1016/j.reactfunctpolym.2022.105209>.
- Pedrazzoli, D., Manas-Zloczower, I., 2016. Understanding phase separation and morphology in thermoplastic polyurethanes nanocomposites. *Polymer* 90, 256–263. <https://doi.org/10.1016/j.polymer.2016.03.022>.
- Pekkanen, A.M., Mondschein, R.J., Williams, C.B., Long, T.E., 2017. 3D printing polymers with supramolecular functionality for biological applications. *Biomacromolecules* 18, 2669–2687. <https://doi.org/10.1021/acs.biomac.7b00671>.
- Rupp, H., Döhler, D., Hilgeroth, P., Mahmood, N., Beiner, M., Binder, W.H., 2019. 3D printing of supramolecular polymers: impact of nanoparticles and phase separation on printability. *Macromol. Rapid Commun.* 40, 1–6. <https://doi.org/10.1002/marc.201900467>.
- Rupp, H., Binder, W.H., 2021. 3D printing of solvent-free supramolecular polymers. *Front. Chem.* 9, 771974 <https://doi.org/10.3389/fchem.2021.771974>.
- Salimi, S., Hart, L.R., Feula, A., Hermida-Merino, D., Touré, A.B.R., Kabova, E.A., Ruiz-Cantu, L., Irvine, D.J., Wildman, R., Shankland, K., Hayes, W., 2019. Property enhancement of healable supramolecular polyurethanes. *Eur. Polym. J.* 118, 88–96. <https://doi.org/10.1016/j.eurpolymj.2019.05.042>.
- Sather, N.A., Sai, H., Sasselli, I.R., Sato, K., Ji, W., Synatschke, C.V., Zambrotta, R.T., Edelbrock, J.F., Kohlmeier, R.R., Hardin, J.O., Berrigan, J.D., Durstock, M.F., Mirau, P., Stupp, S.I., 2021. 3D printing of supramolecular polymer hydrogels with hierarchical structure. *Small* 17, 2005743. <https://doi.org/10.1002/smll.202005743>.
- Shen, M., Bever, M.B., 1972. Gradients in polymeric materials. *J. Mater. Sci.* 7, 741–746. <https://doi.org/10.1007/BF00549902>.
- Smeathers, J.E., Vincent, J.F.V., 1979. Mechanical properties of mussel byssus threads. *J. Molluscan Stud.* 45, 219–230. <https://doi.org/10.1093/oxfordjournals.mollus.a065497>.
- Sunyer, R., Jin, A.J., Nossal, R., Sackett, D.L., 2012. Fabrication of hydrogels with steep stiffness gradients for studying cell mechanical response. *PLoS One* 7, e46107. <https://doi.org/10.1371/journal.pone.0046107>.
- Townsend, J.M., Beck, E.C., Gehrke, S.H., Berkland, C.J., Detamore, M.S., 2019. Flow behavior prior to crosslinking: the need for precursor rheology for placement of hydrogels in medical applications and for 3D bioprinting. *Prog. Polym. Sci.* 91, 126–140. <https://doi.org/10.1016/j.progpolymsci.2019.01.003>.
- Xiao, Y.-Q., Kan, C.-W., 2022. Review on development and application of 3D-printing technology in textile and fashion design. *Coatings* 12, 267. <https://doi.org/10.3390/coatings12020267>.
- Yao, X.F., Liu, D.L., Yeh, H.Y., 2007. Mechanical properties and gradient variations of polymers under ultraviolet radiation. *J. Appl. Polym. Sci.* 106, 3253–3258. <https://doi.org/10.1002/app.26995>.
- Zhou, Z., Samperi, M., Santu, L., Dizon, G., Aboarkaba, S., Limón, D., Tuck, C., Pérez-García, L., Irvine, D.J., Amabilino, D.B., Wildman, R., 2021. An imidazolium-based supramolecular gelator enhancing interlayer adhesion in 3D printed dual network hydrogels. *Mater. Des.* 206, 109792 <https://doi.org/10.1016/j.matdes.2021.109792>.
- Zhu, Y., Tang, T., Zhao, S., Joralmon, D., Poit, Z., Ahire, B., Keshav, S., Raje, A.R., Blair, J., Zhang, Z., Li, X., 2022. Recent advancements and applications in 3D printing of functional optics. *Addit. Manuf.* 52, 102682 <https://doi.org/10.1016/j.addma.2022.102682>.